materials

MDPI

Article

Structural, Elastic, Electronic and Optical Properties of $SrTMO_3$ (TM = Rh, Zr) Compounds: Insights from FP-LAPW Study

Areej M. Shawahni [1], Mohammed S. Abu-Jafar [1,*], Raed T. Jaradat [1], Tarik Ouahrani [2], Rabah Khenata [3], Ahmad A. Mousa [4] and Khaled F. Ilaiwi [1,5]

1 Physics Department, An-Najah N. University, P.O. Box 7, Nablus, Palestine; areeg-92@hotmail.com (A.M.S.); raieddd@hotmail.com (R.T.J.); khaled.ilawi@najah.edu (K.F.I.)
2 Ecole Supérieure en Sciences Appliquées, B.P. 165, Tlemcen 13000, Algeria; tarik.ouahrani@gmail.com
3 Laboratoire de Physique Quantique et de Modélisation Mathématique de la Matière (LPQ3M), Université de Mascara, Mascara 29000, Algeria; khenata_rabah@yahoo.fr
4 Department of Basic Sciences, Middle East University, Amman 11831, Jordan; amousa@meu.edu.jo
5 Department of Basic Sciences, Arab Open University, P.O. Box 4375, Ramallah, Palestine
* Correspondence: mabujafar@najah.edu

Received: 1 September 2018; Accepted: 16 October 2018; Published: 22 October 2018

Abstract: The structural, mechanical, electronic and optical properties of $SrTMO_3$ (TM = Rh, Zr) compounds are investigated by using first principle calculations based on density functional theory (DFT). The exchange-correlation potential was treated with the generalized gradient approximation (GGA) for the structural properties. Moreover, the modified Becke-Johnson (mBJ) approximation was also employed for the electronic properties. The calculated lattice constants are in good agreement with the available experimental and theoretical results. The elastic constants and their derived moduli reveal that $SrRhO_3$ is ductile and $SrZrO_3$ is brittle in nature. The band structure and the density of states calculations with mBJ-GGA predict a metallic nature for $SrRhO_3$ and an insulating behavior for $SrZrO_3$. The optical properties reveal that both $SrRhO_3$ and $SrZrO_3$ are suitable as wave reflectance compounds in the whole spectrum for $SrRhO_3$ and in the far ultraviolet region (FUV) for $SrZrO_3$.

Keywords: perovskite; elastic properties; optical properties; FP-LAPW; mBJ

1. Introduction

Perovskite structure solids are of great interest in materials science due to their simple crystal structure and their different unique properties such as ferromagnetism, ferroelectricity, superconductivity, thermoelectricity and colossal magneto resistance [1]. Recently, many experimental and theoretical works have been devoted to perovskite oxides RE–TM–O_3 (RE represents rare earth and TM represents transition metal elements) [2–4].

$SrTMO_3$ (TM = Rh, Zr) compounds crystallize in the cubic perovskite structure with space group of space *Pm-3m* (# 221). $SrTMO_3$ can be described as Sr^{2+} and O^{-2} ions forming a cubic close packed lattice with TM (Rh, Ti) ions occupying the octahedral holes created by the oxygen. The perovskite structure has a three-dimensional net of corner sharing [TMO_6] octahedral with Sr^{2+} ions in the 12-fold cavities in between the polyhedral [5]. The Sr atom (alkaline earth or rare earth element) is located at (0, 0, 0), the TM atom (transition metal) at (1/2, 1/2, 1/2) and the oxygen atoms sit at face centered positions (1/2, 1/2, 0), (0, 1/2, 1/2) and (1/2, 0, 1/2). A large number of metallic elements are stable in the perovskite structure, if the tolerance factor t is in the range of 0.75–1.0 [6].

The elastic, electronic and optical properties of some perovskite compounds were examined by many researchers [7–10]. In 1992, Roosmalen et al. studied the structure of $SrZrO_3$ [9]. In 2009,

Baudali et al. [10] computed the structural, optical, electronic and thermal properties of $SrTiO_3$ pervoskite cubic structure by using the full potential linearized augmented plane wave (FP-LAPW) method integrated in Wien2k code [11]. In 2011, Daga et al. [12] used the first principle study to calculate the lattice constant of the cubic $SrMO_3$ (M = Ti, Zr, Mo, Rh, Ru). They found the lattice constants of $SrRhO_3$ and $SrZrO_3$ to be 3.932 Å and 4.076 Å, respectively.

In 2016 and 2017, Ali and Rahaman [13,14] used the pseudo potential method integrated in CASTEP code [15] to study the structural, elastic, electronic and optical properties of $SrTMO_3$ (TM = Rh, Mo, Ti, Zr, V) compounds of cubic perovskite. They predicted that $SrTiO_3$, $SrZrO_3$ and $SrVO_3$ have a brittle nature, while $SrMoO_3$ and $SrRhO_3$ have a ductile nature. Moreover, they concluded that $SrRhO_3$ has the highest dielectric constant compared to the other compounds.

$SrZrO_3$ compound (with 4*d*-electrons) is of interest because of its high temperature electronic properties applications such as hydrogen gas sensors and fuel cells. $SrZrO_3$ with high perfection can be grown and used as laser-host materials. Shende et al. [16] suggested that these materials can be used in high-voltage capacitor applications because of their high breakdown strengths and high dielectric constant. $SrRhO_3$ satisfies the conditions for having significant quantum critical fluctuations [17]. A non-Fermi-liquid behavior in transport properties should be observed in $SrRhO_3$ in the range where quantum magnetic fluctuations are active [17]. Considering the heaviness of the band structure, these should be observed in transport [17]. Pseudo gap formation, metal-insulator transitions and high-voltage applications are the other significant properties which draw a considerable attention to 4*d* TMO. To the best of our knowledge, no ab initio investigations of the optical properties of these compounds have been reported and no experimental work on the electronic, elastic and optical properties have been studied too.

In the present work, we have studied the structural, electronic, elastic and optical properties of $SrTMO_3$ (TM = Rh, Zr) by using FP-LAPW (all electron method) method. The motivation of this work is to improve the calculations and to provide some additional information to the features of $SrZrO_3$ and $SrRhO_3$ compounds using the all electron method (FP-LAPW).

2. Computational Details

The computation has been performed by using FP-LAPW method integrated in Wien2k code [11]. In this method, the unit cell is partitioned into two types of regions: (i) atomic-centered muffin-tin (MT) spheres with radius R_α; and (ii) the remaining interstitial region [18]. The expansion of spherical harmonics is defined within a muffin-tin sphere of radius R_{MT} around each nucleus. The Muffin-Tin radius R_{MT} values used are 2.5, 1.95, 1.67 atomic units (a.u) for Sr, Rh and O atoms for the $SrRhO_3$ compound and 2.5, 1.8 and 1.5 a.u for Sr, Zr and O atoms for the $SrZrO_3$ compound. The plane wave cut-off parameter $R_{MT} \times K_{max}$ is equal to 8. The cut-off energy to separate the core states from valence states is set to be -9 Ry. Inside the sphere, Fourier expanded up to $G_{max} = 14$ with a cut-off $l_{max} = 12$ and 35 k-points in the irreducible Brillion zone with a grid of $10 \times 10 \times 10$ Monkhorst-Pack meshes [19] (equivalent to 1000 k points in full Brillion zone) which are used to obtain self-consistency for $SrRhO_3$ and $SrZrO_3$ compounds to be better than 0.1 mRy. The Perdew-Burke-Ernzerhof–generalized gradient approximation (PBE-GGA) is used for the exchange correlation potential [20], while the modified Becke-Johnson potential (mBJ-GGA) [21] is also used to improve the energy band gap of the herein studied compounds.

3. Results and Discussions

3.1. Structural Properties

Strontium Transition metal oxides ($SrTMO_3$) crystallize in the ABO_3 cubic perovskite structure with the space group *Pm-3m* (221). The crystal structure of $SrTMO_3$ (TM = Rh, Zr) is shown in Figure 1. We have optimized the lattice parameters (a) of these compounds by minimizing the total energy. The total energy at different unit cell volumes for $SrTMO_3$ (TM = Rh, Zr) is shown in Figure 2,

the volume versus energy is fitted to the Murnaghan equation of state [22] to estimate the ground-state properties of these compounds such as the lattice constant (a), the bulk modulus (B) and the pressure derivatives of the bulk modulus (B'). These obtained values are listed in Table 1 together with the available experimental and theoretical data for comparison. In general, the computed structural parameters are in good agreement with experimental and theoretical data available in the literature. More precisely, the lattice parameters of $SrRhO_3$ and $SrZrO_3$ are found to be 3.976 Å and 4.176 Å, respectively. The present calculations show that the lattice parameter of $SrRhO_3$ ($SrZrO_3$) is 1.43% (1.63%) larger than the experimental value [23,24]. This guarantees the reliability of the present first-principles computations for the lattice parameters of these compounds using the PBE-GGA method. The calculated bulk modulus for $SrZrO_3$ is 2.11% larger than the experimental value [25].

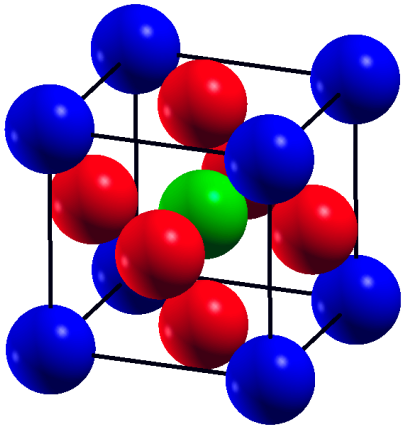

Figure 1. The crystal structure of $SrTMO_3$ (TM = Rh, Zr), (blue spheres are Sr atoms, red spheres are Oxygen O atoms and green spheres are TM atoms).

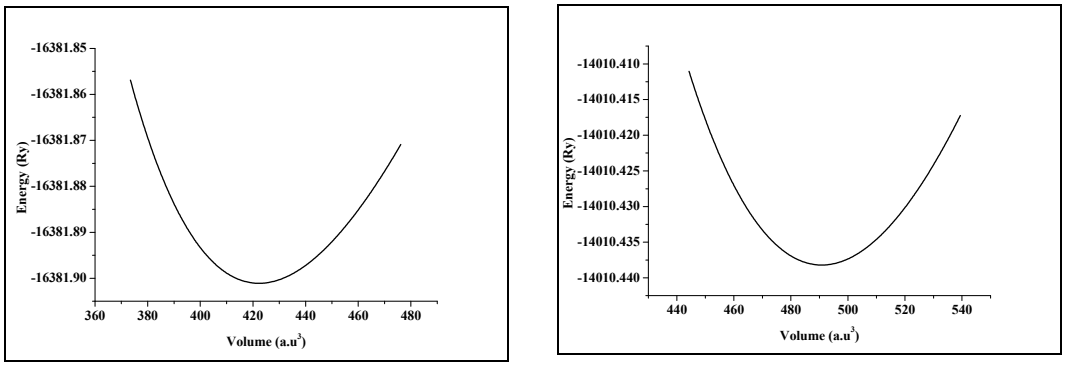

(**a**) (**b**)

Figure 2. Total energy as a function of the volume of (**a**) $SrRhO_3$ compound and (**b**) $SrZrO_3$ compound.

Table 1. Calculated lattice parameter (a), bulk modulus (B), first pressure derivative (B') of $SrTMO_3$ (TM-Rh, Zr).

Compound		a (Å)	B (GPa)	B'
$SrRhO_3$	Present work	3.976	162.55	5.97
	Experimental work	3.92 [23]	–	–
	Other theoretical work	3.932 [12] 4.074 [14]	–	–
$SrZrO_3$	Present work	4.176	153.25	3.98
	Experimental work	4.109 [24]	150 [25]	–
	Other theoretical work	4.076 [12] 4.177 [14]	–	–

3.2. Electronic Properties

In this section, we study the electronic properties of $SrRhO_3$ and $SrZrO_3$ via calculating the energy band structure and density of states. The calculated band structures along the high symmetry lines in Brillion-zone of $SrRhO_3$ and $SrZrO_3$ at zero pressure using PBE-GGA approximation [20] are depicted in Figure 3, where the Fermi level is set at zero eV. In $SrZrO_3$, the valence band maximum (VBM) occurs along the M-point symmetry line, while the conduction band minimum occurs along the Γ-point symmetry line with energy band gap 3.69 eV, resulting in an indirect energy band gap (M-Γ) semiconductor.

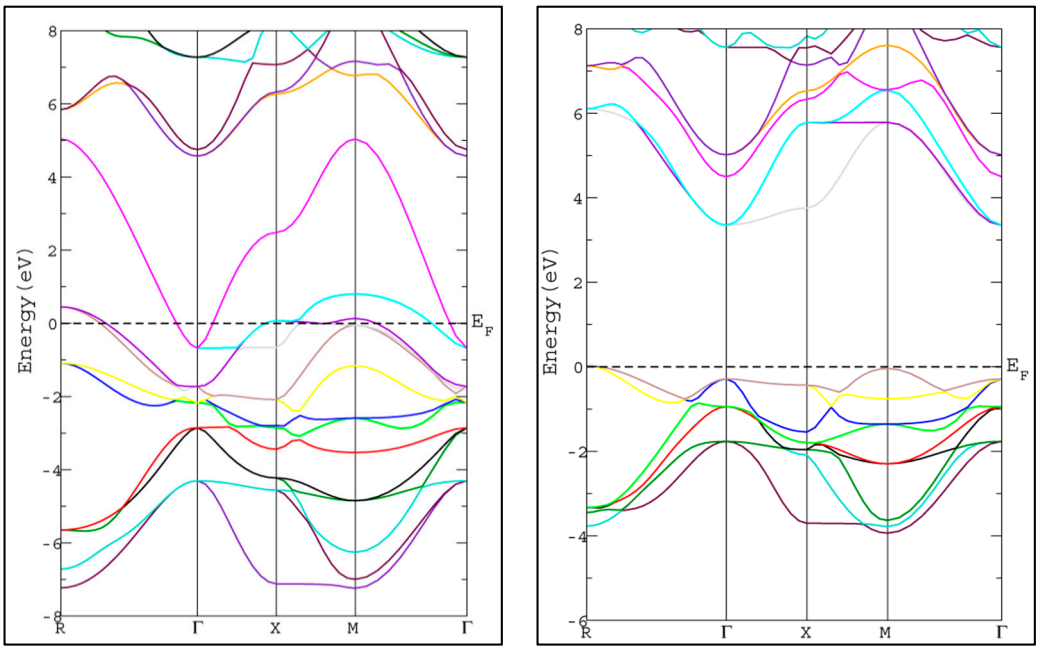

Figure 3. Band structure of cubic pervoskite using PBE-GGA method for (**a**) $SrRhO_3$ and (**b**) $SrZrO_3$ compounds.

The calculated energy band gap is tabulated in Table 2 along with the available previous theoretical value [26]. The calculated energy gap is larger than the theoretical value by 0.32 eV [26]. To the best of our knowledge, there is no experimental value available to compare with. The usual trend of the modified Becke-Johnson potential (mBJ-GGA) method is enlarging the energy band gap values (E_g) of the semiconductor and insulator materials which makes E_g comparable to the experimental results [21]. The band structures of $SrRhO_3$ and $SrZrO_3$ compounds using mBJ-GGA are displayed in Figure 4. For the $SrZrO_3$ compound, the minimum energy gap within mBJ-GGA is still indirect with the same direction as the PBE-GGA approach, but its value increases by about 0.85 eV to become 4.54 eV. $SrZrO_3$ is classified as an insulator within the mBJ-GGA method. $SrRhO_3$ has a metallic nature with no energy gap within the two approaches PBE-GGA and mBJ-GGA.

Table 2. Calculated energy band gap E_g (eV) of $SrZrO_3$ compound.

Present Work		Other Theoretical Work
PBE-GGA	**mBJ-GGA**	
3.69 eV	4.53 eV	3.37 eV [26]

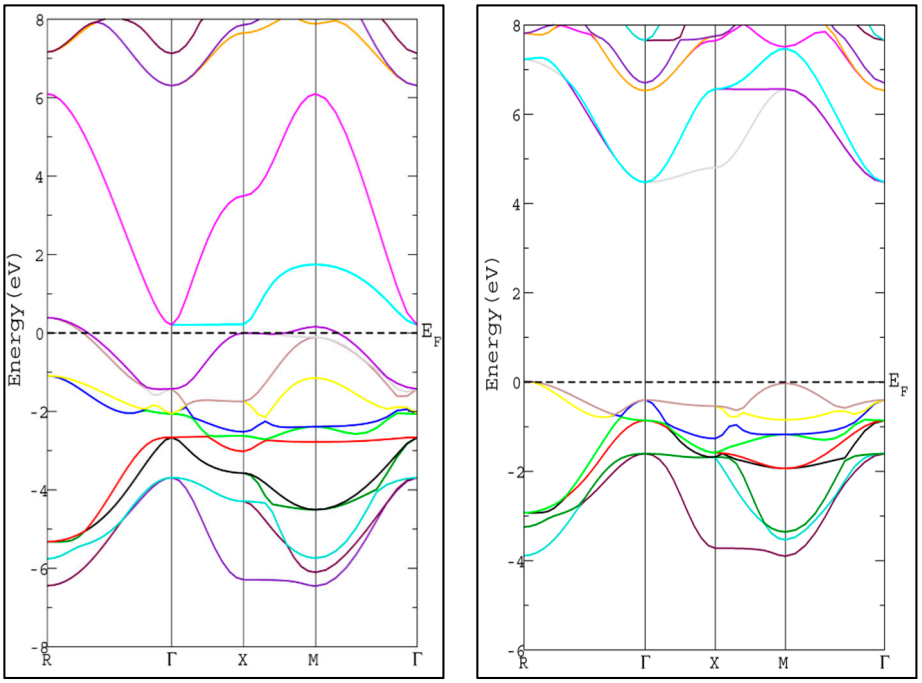

(**a**) (**b**)

Figure 4. Band structure of cubic pervoskite (**a**) $SrRhO_3$ and (**b**) $SrZrO_3$ by using (mBJ-GGA) method.

The total and partial density of states for $SrRhO_3$ and $SrZrO_3$ are shown in Figures 5 and 6 for an energy range from −15 to 14 eV and −12.5 to 14 eV, respectively. In $SrRhO_3$, the valence band originates from O-*p* and Rh-*d* states. The maximum contribution of the Rh-*d* state is near the Fermi level. In the conduction band, the bands are due to the Sr-*d* with a small contribution from Rh-*d*, O-*p* and O-*s* states. In SrZrO3, the valence band originates from O-*p* with few contribution from Zr-*d*,*p* and Sr-*d* states. In the conduction band, the bands are due to Zr-*d* and Sr-*d* states with a small contribution from O-*p* states.

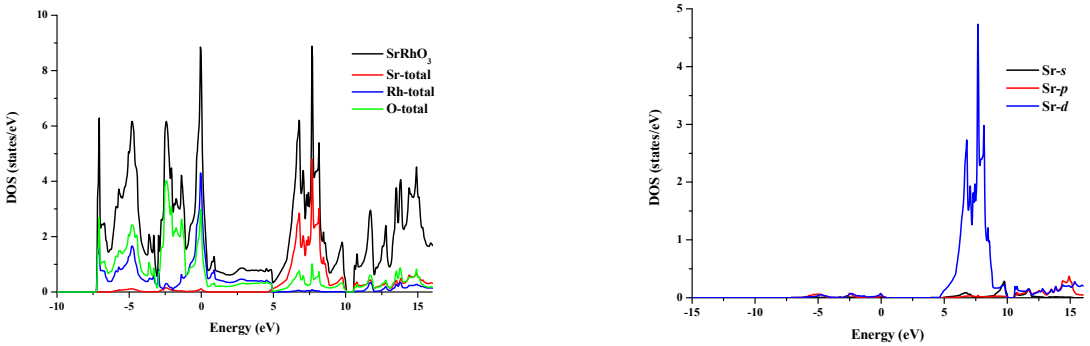

(**a**) (**b**)

Figure 4. *Cont.*

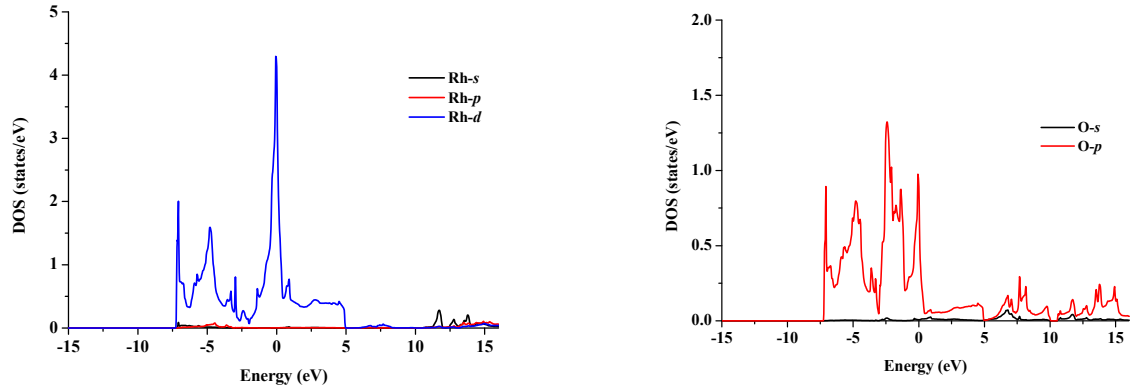

Figure 5. (**a**) Total density of states of $SrRhO_3$ compound and partial density of states for (**b**) Sr atom, (**c**) Rh atom and (**d**) O atom in $SrRhO_3$ compound.

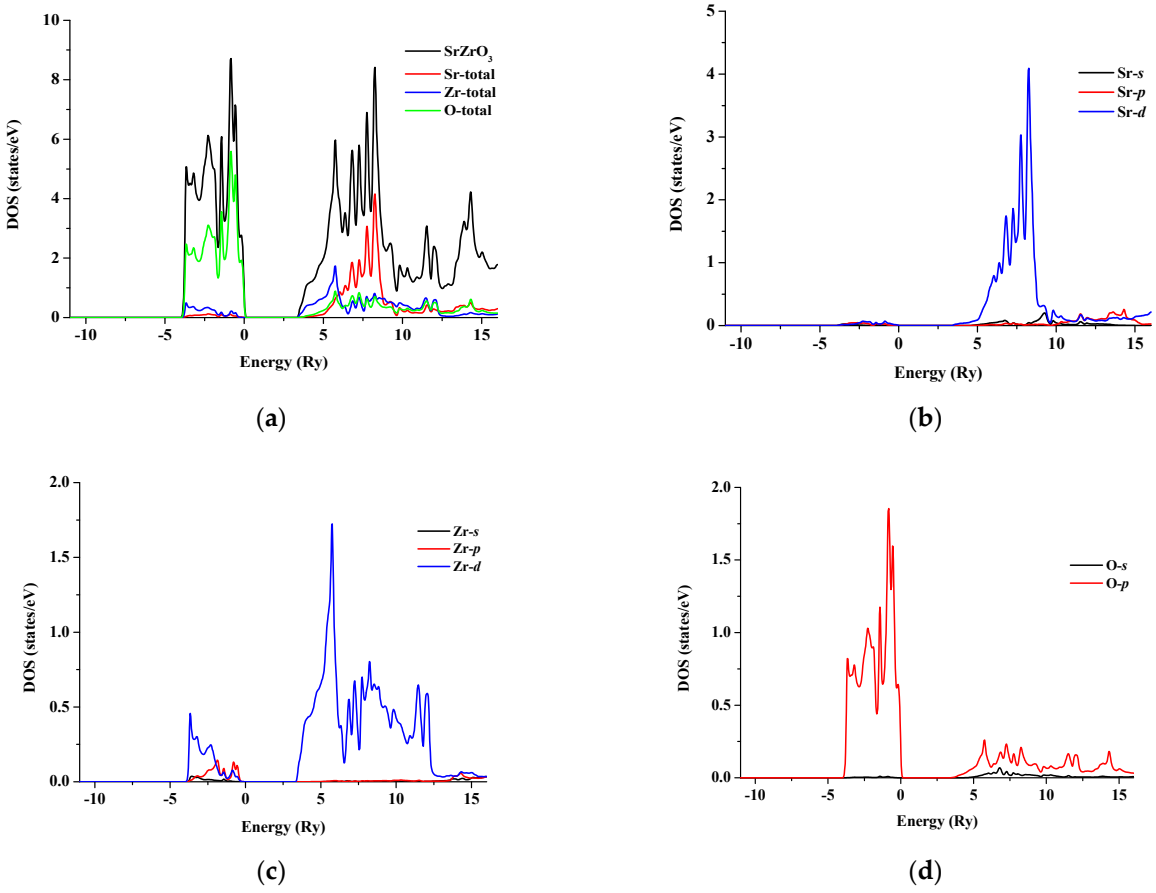

Figure 6. (**a**) Total density of states of $SrZrO_3$; Partial density of state for (**b**) Sr atom, (**c**) Zr atom and (**d**) O atom in $SrZrO_3$ compound.

To make a deeper analysis of the bonding nature of our titled compounds, the wave function obtained from a final Wien2k calculation at the optimal geometry has been analyzed in the critic program (version 1.0). Critic is a full-edged program for the topological analysis of solid-state electron densities.

This program uses the quantum theory of atom in molecule (QTAIM) to make a topological analysis of the electronic density (ϱ) of a crystal. By means of QTAIM, we can automatically locate all critical points (CP's) of the electronic density rising from a nil flux of the electron density gradient

condition [27]. The procedure implemented in critic is to divide ϱ into disjoint regions Ω (basins) through the real space approaches. Here, we can generate topological schemes in two or tridimensional plots. It is clearly shown from the topological distribution of the charge density in Figure 7A, that the charge distribution in the $SrZrO_3$ compound is spherically symmetrical. This suggests that all electronic charges are localized around anions—a typical ionic bonding. The same trend is also displayed for the second compound with some small difference in the distribution of ϱ due to the charge transfer, which differs in the two titled compounds (see Figure 7C). We also present in Figure 7B,D, the molecular graph of our two perovskites.

These plots were done following the character of Wyckoff's, bond CP and ring CP family [28]. The form of the atomic basin generated by the CCP point suggests that both $SrRhO_3$ and $SrZrO_3$ are belonging to the R11 family (see Figure 7B,D) [28]. Here, we can define a topological charge of each atomic basin. As results, Q(Sr) = 1.59 electron, Q(Rh) = 1.47 electron and Q(O) = −1.05 electron for $SrRhO_3$, and Q(Sr) = 1.61 electron, Q(Zr) = 2.49 electron and Q(O) = −1.37 electron for the $SrZrO_3$ compound. When we compare these charges with the oxidation number corresponding to each of the atoms, we find that the charge transfer is mainly due to the strontium one, with an equal percentage of 80% in both perovskites. However, we note that replacing the cation Rh with electro-negativity of 2.2 by the Zr one with low electro-negativity of 1.4 has a negligible effect on the nature of the bonding. The $SrZrO_3$ has a more ionic trend. However, even the constituent cations show different charge transfer (Zr and Rh are transferred by 62% and 37%) and each of them varies as strongly as the oxide ions. The latter adapt their charges according to electro-neutrality requirements. There is a second topological index that has been proposed as a global measurement of the degree of metallicity, the electron density flatness defined as $f = \frac{\rho_c^{\min}}{\rho_b^{\max}}$ where $\rho_c^{\min}$ is the minimal electron density found on the unit cell (it necessarily corresponds to a critical point) and $\rho_b^{\max}$ is the maximal electron density among bond critical points. This flatness has values close to one on common metallic compounds and close to zero on localized bonding compounds [29]. The delocalization of electrons (flatness) in the $SrRhO_3$ and $SrZrO_3$ compounds are respectively equal to 80.61% and 5.62%. This suggests that the global chemical behavior of $SrRhO_3$ is metallic, whereas $SrZrO_3$ is nonmetallic. To go further in the characterization of the bonds nature of the titled compounds we have employed another tool named the electron localization function (ELF) [30], which is based on a measure of the likelihood of finding an electron in the neighborhood space of a reference electron located at a given point and with the same spin. Taking into account that the homogeneous electron gas has an ELF value of 0.5, valence electrons of metals should deviate very slightly from this quantity. The ELF isosurfaces, as well as the one-dimensional projections of Sr–O–Rh and Sr–O–Zr bond paths of the investigated perovskites are depicted in Figure 8. It is strikingly clear from the plot that O–Zr and O–Rh are different. The integration of population on the ELF attractor of the $SrZrO_3$ compound shows two types of Zr–O bonds, the first one has ELF maxima equal to 0.78 and the second to 0.83; the former has the negligible population, but the latter has 0.95 electrons. The integration gives a number of the delocalized attractor as lone pair bonds around the Sr and Zr cations; the population in this attractor varies from 1.4 to 1.1 electrons. Regarding the second compound ($SrRhO_3$), no O–Rh bonds have been found, only delocalized lone pair ones with ELF maxima near to 0.5 are reported. Here, we should emphasize that the delocalization of these attractors in the $SrRhO_3$ compound provides a reliable measure of the delocalization of wave function and its localization in the $SrZrO_3$ compound.

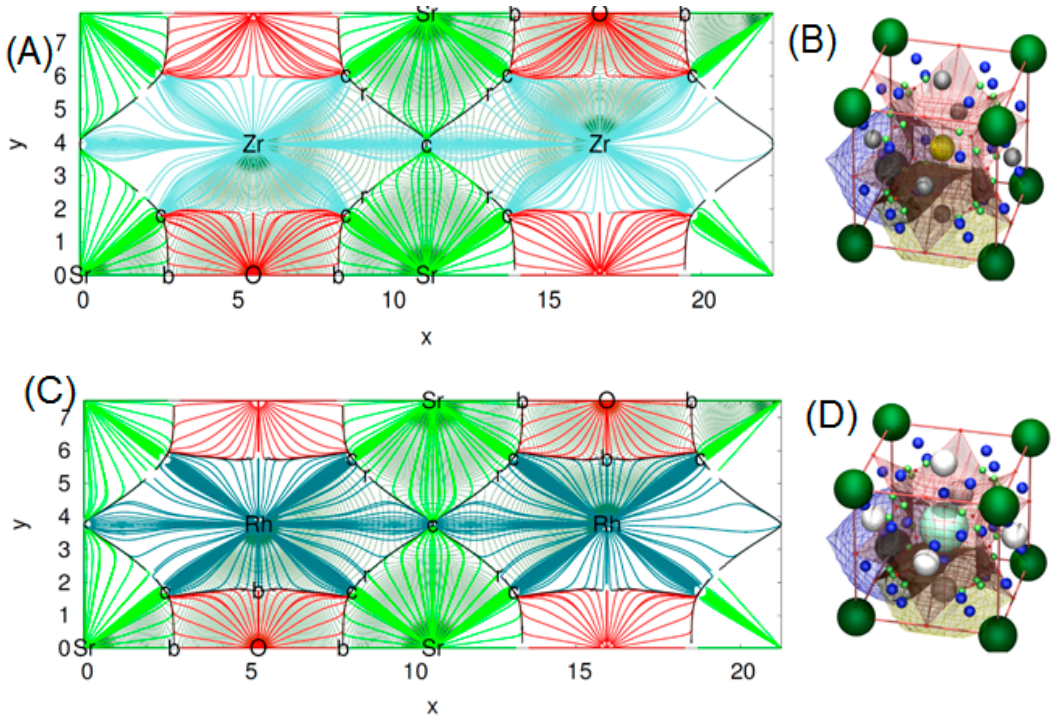

Figure 7. 2D map of topological analysis of electron density of (**A**) $SrZrO_3$ and (**C**) $SrRhO_3$, molecular graph representation of (**B**) $SrZrO_3$ and (**D**) $SrRhO_3$. In colored trajectories traced out by the electron density gradient, vector field (in electron/bohr^3) of upper panel: $SrZrO_3$ and lower panel: $SrRhO_3$ are at their denser plane. Here, the red, dark blue, light blue and green lines refer respectively to O, Rh, Zr and Sr atomic basins. The set of trajectories that terminates at each bond's critical point (b) defines an interatomic surface. The set of trajectories that originate at the ring critical (r) point defines the perimeter of the interatomic surface. The gradient paths associated with the negative eigenvalues at the (n) point terminate at this CP and define the zero-flux surfaces that partition the crystal into unique fragments (the atomic basins). On the right of the figures, molecular graph representation: the small red balls placed at the Wyckoff's 3c are the r CPs. The light green balls the b CPs and the dark blue the c cage CPs.

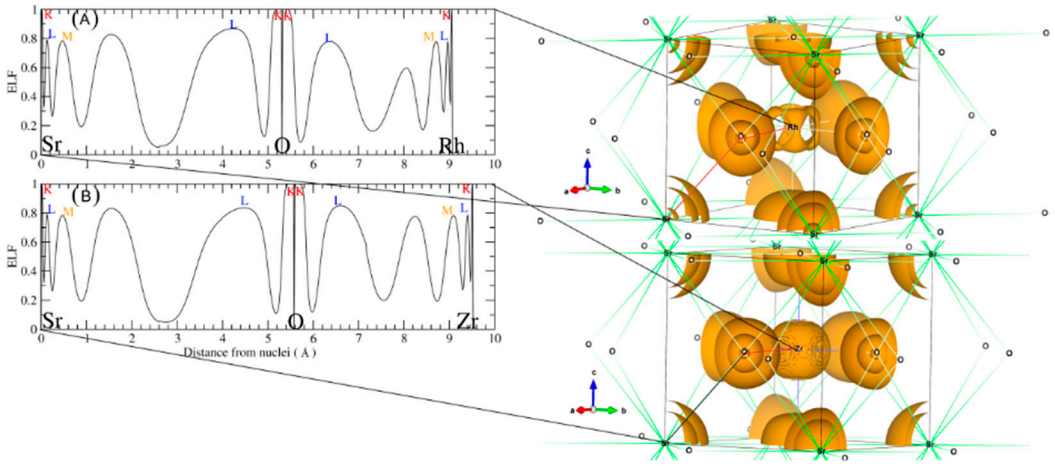

Figure 8. Left panel shows a one dimensional electron localization profile and the right panel shows the 3D isosurface of ELF basins of (**A**) $SrRhO_3$ and (**B**) $SrZrO_3$ compounds.

3.3. Elastic Properties

In this subsection, we turn our attention to study the mechanical properties of $SrRhO_3$ and $SrZrO_3$ via calculating their elastic constants. These constants define the properties of material that undergo stress, deform and then recover, returning to its original shape after stress ceases. They have a significant role in finding information about the brittleness, ductility, stiffness and the mechanical stability of the material [31]. The elastic constants require knowledge of the derivative of the energy as a function of the lattice strain. In the case of the cubic system, this strain is chosen in such a way that the volume of the unit cell is preserved. Thus, for the calculation of elastic constants C_{11}, C_{12} and C_{44}, for these compounds we have used the method developed by Morteza Jamal [32] and integrated in Wien2k code as the IRelast package (Cubic-elastic_13.2). The calculated C_{ij} constants are listed in Table 3. Our computed C_{ij} data are in reasonable agreement with previous theoretical results. In view of Table 3, it can be noticed that the calculated values of the elastic modulus C_{11}, which are related to the unidirectional compression along the principal crystallographic directions, are much higher than that of C_{44}, which represent the resistance to the shear deformation, indicating the weak resistance to the shear deformation compared to the resistance to the unidirectional compression. The mechanical stability of a cubic material requires that its independent elastic constants should satisfy the following Born's stability criteria [33,34]:

$$C_{11} > 0; C_{44} > 0; C_{11} + 2C_{12} > 0; C_{11} > B > C_{12} \quad (1)$$

From Table 3, we can see that all required conditions given in the above Equation (1) are simultaneously satisfied, which clearly indicates that the $SrRhO_3$ and $SrZrO_3$ are mechanically stable.

The three elastic constants C_{11}, C_{12} and C_{44} are estimated from first-principles calculations for $SrRhO_3$ and $SrZrO_3$ single-crystals. However, the prepared materials are in general polycrystalline, and therefore it is important to evaluate the corresponding moduli for the polycrystalline species using the Hill's approach [35]. In this approach, the effective modulus for polycrystals could be approximated by the arithmetic mean of the two well-known bounds for monocrystals according to Voigt [36] and Reuss [37]. Then, for the cubic system, the shear modulus S in the mentioned approximations: Voigt (V), Reuss (R) and Hill (H) are calculated from the elastic constants of the single crystal, in the following form:

$$\begin{aligned} S_V &= \frac{1}{5}(C_{11} - C_{12} + 3C_{44}) \\ S_R &= \frac{5C_{44}(C_{11} - C_{12})}{4C_{44} + 3(C - C_{12})} \\ S_H &= \frac{1}{2}(S_v + S_R) \end{aligned} \quad (2)$$

To compute the Young's modulus (Y), Poisson's ratio (ν), and the anisotropic factor (A), the following equations are used, respectively:

$$Y = \frac{9S_H B}{(S_H + 3B)} \quad (3)$$

$$v = \frac{3B - 2S_H}{2(3B + S_H)} \quad (4)$$

$$A = \frac{2C_{44}}{C_{11} - C_{12}} \quad (5)$$

The computed bulk modulus, shear modulus, Young's modulus, Poisson's ratio and anisotropic factor are listed in Table 3 along with the theoretical results [14,38]. The bulk modulus and shear modulus can be used to measure the material hardness [39]. In general, when S_H values increase,

the materials become stiffer. From the obtained values of shear modulus S_H one can remark that $SrZrO_3$ is stiffer than $SrRhO_3$.

Table 3. Calculated elastic constants of $SrTMO_3$ (TM = Rh, Zr).

Compound		C_{11}	C_{12}	C_{44}	B	S_H	B/S_H	Y	ν	A
$SrZrO_3$	Present work	319.61	72.54	88.05	154.90	102.2	1.52	248.62	0.23	0.71
	Theory [38]	338.60	71.00	77.00	160.00	118.8	1.35	247.64	0.20	0.58
	Theory [14]	299.16	72.57	72.58	124.76	74.81	1.67	241.34	0.25	0.64
$SrRhO_3$	Present work	239.53	131.17	100.27	167.29	78.32	2.14	203.25	0. 30	1.85
	Theory [14]	196.25	99.9	46.28	132.01	47.02	2.81	126.11	0.34	0.96

To categorize the brittle and ductility behaviors of a material, the ratio of the bulk modulus to the shear modulus, B/S, an empirical relationship related to the plastic and elastic properties of the material, is used. According to Pugh [40], a high B/S value is associated with ductility, while a low value is consistent with brittleness. The critical value that separates the two behaviors has been determined to be 1.75. The results listed in Table 3 clearly indicate that the $SrRhO_3$ ($SrZrO_3$) compound has B/S_H ratio higher (smaller) than the critical value of 1.75, which classifies $SrRhO_3$ ($SrZrO_3$) compound as ductile (brittle) material. In addition, to identify the materials as ductile or brittle, we also applied the Cauchy's pressure rule defined as the difference between the elastic constants C_{12}–C_{44} [41]. According to this rule, if the Cauchy's pressure is positive (negative), the material will be ductile (brittle) in nature. As shown in Table 3, It is seen that the Cauchy's pressure is positive for $SrRhO_3$ and negative for $SrZrO_3$, confirming the ductile nature for $SrRhO_3$ and the brittle behavior for the $SrZrO_3$ compound. We may also refer to Frantsevich et al. [42] who distinguishes the ductility and brittleness of materials in terms of Poisson's ratio (ν). According to this rule, if the Poisson's ratio is less than 0.26, the material will be brittle in nature; otherwise, the material will be ductile. As shown, the computed Poisson's ratiosare 0.30 for $SrRhO_3$ and 0.23 for $SrZrO_3$, categorizing $SrZrO_3$ as brittle compounds and $SrRhO_3$ as ductile compounds. These results exactly agree with the results of the B/S ratio and Cauchy's pressure.

The anisotropy factor is an important parameter to measure the degree of materials anisotropy; also, it has a significant usage in engineering science to inspect the potential of micro-cracks in the material [43,44]. For completely isotropic materials, the anisotropy factor A takes the value of the unity and the deviation from unity measures the degree of elastic anisotropy. The calculated values of the anisotropic factor A are found to be equal to 1.85 for $SrRhO_3$ and 0.71 for $SrZrO_3$, suggesting that both compounds are anisotropic in nature and $SrRhO_3$ is characterized by a profound anisotropy.

3.4. Optical Properties

Since the investigated compounds have cubic symmetry, we need to calculate only one dielectric tensor component to completely characterize their linear optical properties. The frequency-dependent complex dielectric function $\varepsilon(\omega) = \varepsilon_1(\omega) + i\varepsilon_2(\omega)$; where $\varepsilon_1(\omega)$ and $\varepsilon_2(\omega)$ are the real and imaginary components of the dielectric function, respectively; is known to describe the optical response of the medium at all photon energies $E = \hbar\omega$, using the formalism of Ehrenreich and Cohen [45].

Complex dielectric function can be derived from the definition given by Hedin [46]

$$\epsilon(r,t,r',t') = \delta(r-r')\delta(t\ -\ t')\ -\int P(r,t,r'',t')v(r''\ -\ r')dr'' \tag{6}$$

where P is the polarization propagator and is the Coulomb interaction; P can be given by the following form:

$$P(\omega,q) = \frac{1}{V}\sum_{n',n,k}\frac{f_0\left(\varepsilon_{n,k+q}\right)\ -\ f_0\left(\varepsilon_{n',k}\right)}{\varepsilon_{n,k+q}\ -\ \varepsilon_{n',k}\ -\ W}\left|M_{n,n'}(k,q)\right|^2 \tag{7}$$

where V is the unit cell volume, f_0 is the Fermi distribution function and ε_k is the single particle energy. The matrix element can be given by: $M_{n,n'}(k,q) = \langle\, u_{nk} \,|\, e^{-iq,r} \,|\, u_{n'k} \,\rangle$, q is the wave vector of light and it is much smaller than the wave vector of electrons in the system; the matrix elements $M_{n,n'}(k,q)$ with small q can be given by:

$$M_{m,n}(k,0) = \delta_{l,n} - (\delta_{l,n} - 1)\frac{h\, P_{m,n,k}}{2\pi(\varepsilon_{n,k} - \varepsilon_{m,k})}\, q \tag{8}$$

The sum over n' and n must be split into two terms, one with $n' = n$ corresponding to intra-band electronic transitions, and the second with $n' \neq n$, corresponding to inter-band transitions, the intra-band part of the dielectric function $\epsilon(\omega,0)$ can be given by:

$$\epsilon^{\text{intra}}(\omega,0) = 1 - lim_{q\to 0}\frac{4\pi e^2}{V|q|^2}\sum_{n,k}\frac{f_0\left(\varepsilon_{n,k+q}\right) - f_0(\varepsilon_{n,k})}{\varepsilon_{n,k+q} - \varepsilon_{n,k} - \omega}|M_{n,n}(k,q)|^2 \tag{9}$$

while the inter band part can be written as

$$\epsilon^{\text{inter}}(\omega,0) = -lim_{q\to 0}\frac{4\pi e^2}{V|q|^2}\sum_{n,n',k}\frac{f_0\left(\varepsilon_{n',k+q}\right) - f_0(\varepsilon_{n,k})}{\varepsilon_{n',k+q} - \varepsilon_{n,k} - \omega}|M_{n,n'}(k,q)|^2 \tag{10}$$

where $n' \neq n$ in Equation (10).

The imaginary part of the $\varepsilon(\omega)$ in the long wavelength limit has been obtained directly from the electronic structure calculation, using the joint density of states (JDOS) and the transition moments elements $M_{n,n'}(k,q)$:

$$\varepsilon_2(\omega) = \frac{e^2\hbar}{\pi m^2\omega^2}\sum_{v,c}\int_{BZ}\left|M_{n,n'}(k,q)\right|^2\delta\left[\omega_{n,n'}(k) - \omega\right]d^3k \tag{11}$$

The integral is over the first Brillouin zone. The real part of $\varepsilon(\omega)$ can be derived from the imaginary part using the Kramers–Kronig relations.

$$\varepsilon_1(\omega) = 1 + \frac{2}{\pi}P\int_0^\infty \frac{\omega'\varepsilon_2(\omega')}{\omega'^2 - \omega^2}\mathrm{d}\omega' \tag{12}$$

where P implies the principal value of the integral. The knowledge of the real and imaginary parts of the dielectric function allows the calculation of other important optical functions such as the refractive index $n(\omega)$, reflectivity $R(\omega)$, extinction coefficient $k(\omega)$, energy loss function $L(\omega)$ and absorption coefficient $\alpha(\omega)$ by using the following expressions [47–49]:

$$n(\omega) = \left(\frac{1}{2}\left[\sqrt{\varepsilon_1^2(\omega) + \varepsilon_2^2(\omega)} + \varepsilon_1(\omega)\right]\right)^{\frac{1}{2}} \tag{13}$$

$$R(\omega) = \left|\frac{\sqrt{\varepsilon(\omega)} - 1}{\sqrt{\varepsilon(\omega)} + 1}\right|^2 = \left|\frac{\sqrt{\varepsilon_1 + i\varepsilon_2} - 1}{\sqrt{\varepsilon_1 + i\varepsilon_2} + 1}\right|^2 \tag{14}$$

$$k(\omega) = \left(\frac{1}{2}\left[\sqrt{\varepsilon_1^2(\omega) + \varepsilon_2^2(\omega)} - \varepsilon_1(\omega)\right]\right)^{\frac{1}{2}} \tag{15}$$

$$\mathrm{L}(\omega) = \frac{\varepsilon_2(\omega)}{\varepsilon_1(\omega)^2 + \varepsilon_2(\omega)^2} \tag{16}$$

$$\alpha(\omega) = \frac{\sqrt{2}\omega}{c}\left(\sqrt{\varepsilon_1^2(\omega) + \varepsilon_2^2(\omega)} - \varepsilon_1(\omega)\right)^{\frac{1}{2}} \quad (17)$$

Real and imaginary parts of the dielectric constant are displayed in Figure 9a–d for the $SrRhO_3$ compound. The value of the static real part of the dielectric function $\varepsilon_1(0)$ for the $SrRhO_3$ compound within intra and inter band transition in Figure 9a is negative, while the imaginary part of the static dielectric function $\varepsilon_2(0)$ within intra and inter band transition Figure 9c is positive; this implies two important facts: Firstly, the $SrRhO_3$ compound has considerable metallic behavior, which agrees with the energy band structure calculations. Secondly, the negative value of (ε_1) especially in the energy range 0–1.15 eV in Figure 9a and the highly positive value of $\varepsilon_2(\omega)$ at the early beginning of Figure 9c, reveal the loss of light transit. Real dielectric constant within intra band transition for $SrRhO_3$ in Figure 9b has small peaks; the first two of them are centered at 1.42 eV and 3.73 eV. We see that (ε_1) for the $SrRhO_3$ compound in Figure 9a, it has roots in the 1.15 eV, 1.55 eV, 5.0 eV, 8.45 eV and 13.5 eV. When these roots occur, (ε_1) = 0, the compound does not respond to incident light, this fact is mainly due to the Plasmon oscillation. The sharp increase in $\varepsilon_1(\omega)$ with intra and inter band transition, in Figure 9a, at an energy range 0–1.15 eV, indicates that the compound does not interact with the incident photons at this energy range. The static dielectric constant $\varepsilon_1(0)$ of $SrRhO_3$ with inter + intra in Figure 9a and intra band transition Figure 9b are −180 and 32, respectively. Negative value $\varepsilon_1(0)$ of with inter + intra band transition ensures the metallic behavior of $SrRhO_3$ compound. By taking only the intra band transition into account as seen in Figure 9b,d, both the real and imaginary parts of dielectric constant have positive values, which indicates a mix of metallic and semiconducting behavior for the $SrRhO_3$ compound. This implies that for metallic compounds inter and intra band transitions must be taken into account.

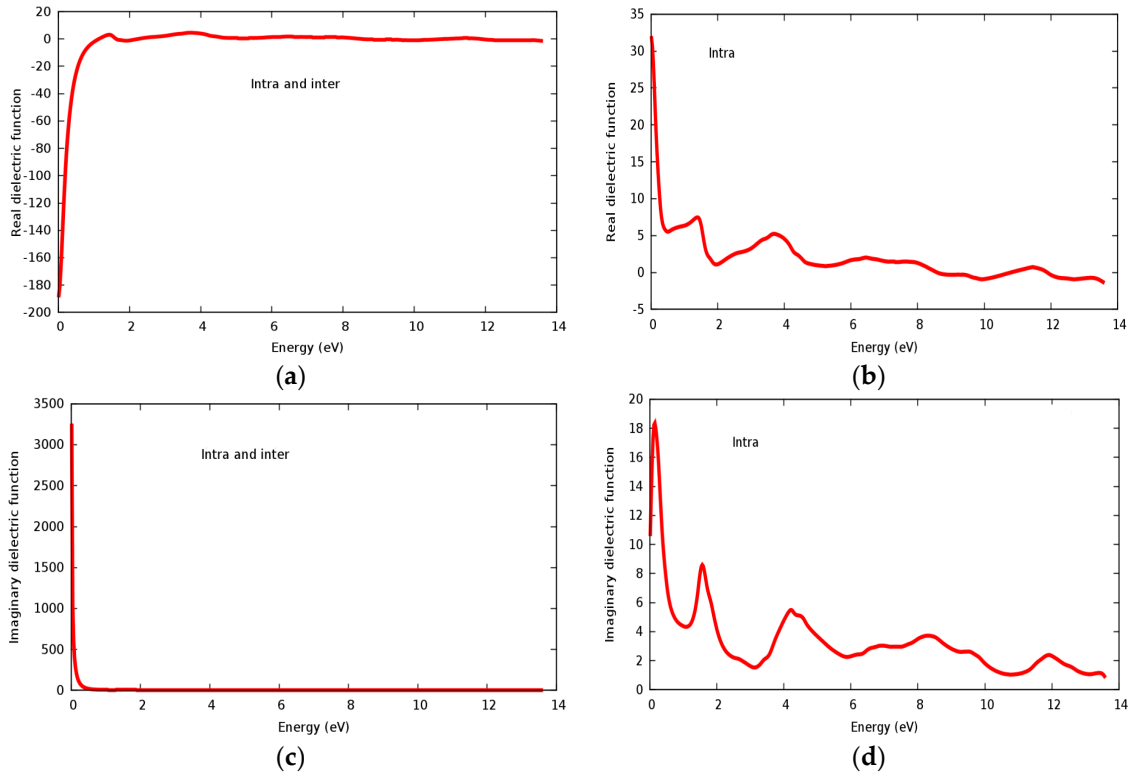

Figure 9. The dielectric function of $SrRhO_3$ compound: (**a**,**b**) Real part; (**c**,**d**) Imaginary part.

Optical conductivity is a quantity depending on the inter band and intra band transitions. In Figure 10a,b, the real and imaginary parts of conductivity are illustrated for the $SrRhO_3$ compound, by taking the inter and intra band transition into account; the static real conductivity is high, while it

is zero when only intra band transition is taken into account. As the incident light energy increases, the real and imaginary parts of conductivity with the two approaches; intra + inter and intra band transition; both almost have the same behavior.

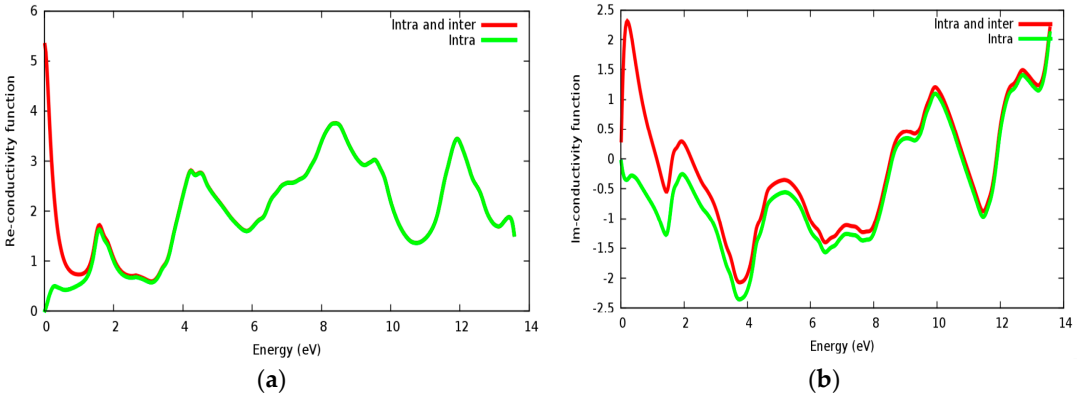

Figure 10. The conductivity function of $SrRhO_3$ compound: (**a**) Real part; (**b**) Imaginary part.

The refractive index $n(\omega)$ and extinct factor $k(\omega)$ for the $SrRhO_3$ compound are illustrated in Figure 11a,b and Figure 12a,b, respectively. The $SrRhO_3$ has a high $n(0)$ and $k(0)$ with intra and inter band transition, which indicates metallic behavior for the real and imaginary parts of the dielectric. As the incident light energy increases the $n(\omega)$; and $k(\omega)$ goes to a lower values. Many peaks are shown in $n(\omega)$ and $k(\omega)$ spectra, these peaks originate from intra-band transition. The extinction coefficient depends on the amount of absorption of the photon when it propagates in the material, while the refractive index indicates the phase velocity of the electromagnetic wave.

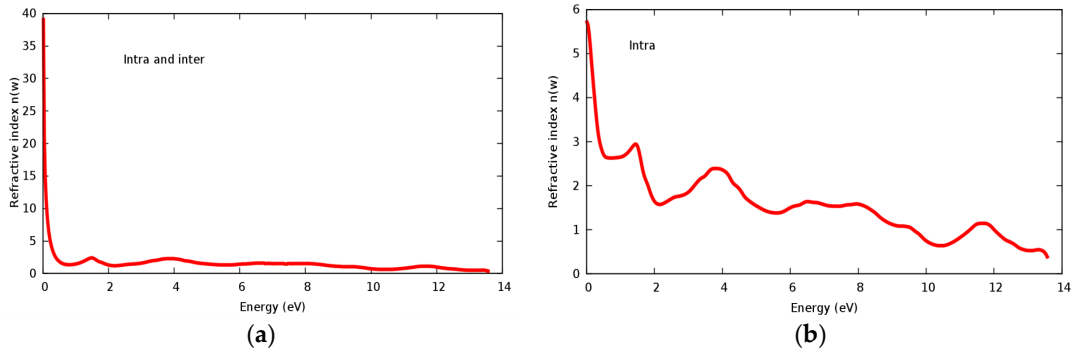

Figure 11. (**a**) Refractive index $n(\omega)$ within inter and intra; (**b**) Refractive index $n(\omega)$ within intra for $SrRhO_3$ compound.

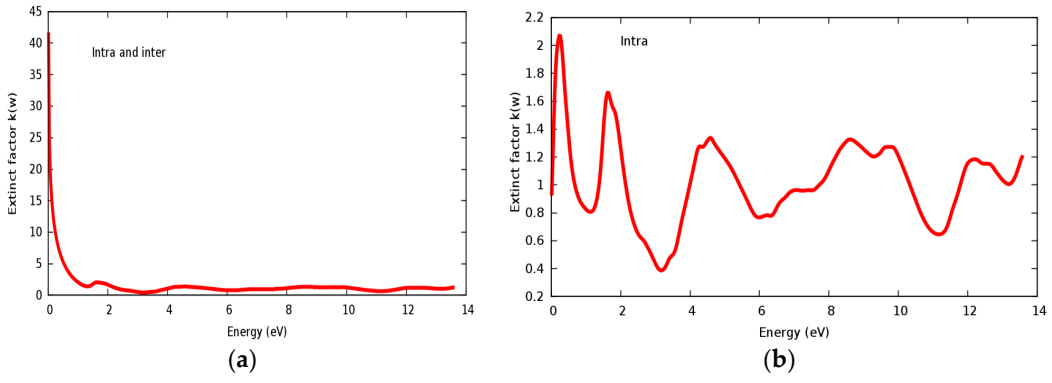

Figure 12. (**a**) Extinct factor $k(\omega)$ within inter and intra; (**b**) Extinct factor $k(\omega)$ within intra for $SrRhO_3$ compound.

The reflectivity spectra of $SrRhO_3$ as a function of energy are shown in Figure 13a. The static reflectivity of $SrRhO_3$ within intra and inter transition is 0.95, while it is 0.5 within intra transition. The reflectivity of $SrRhO_3$ in the low energy region goes down as the incident light energy increases, while it increases in the high energy region—the far ultraviolet region (FUV). The absorption coefficient spectra of $SrRhO_3$ is plotted in Figure 13b, absorption spectra, as shown, begins at the early beginning and increases as the incident photon energy increases with some peaks along the spectrum. The observed peaks in the spectra related to electron transitions from conduction to valence bands, sharp peaks in the absorption spectrum may be accordance with transitions between valance and conduction band (inter band transitions) that can be considerably far from each other. The $SrRhO_3$ compound is a good absorbent compound because it is a metal compound and it is identical with intra + inter and intra band transition. Peaks in the spectrum of the absorption coefficient are proportional to the peaks in the (ε_2) spectrum. The energy loss function $L(\omega)$ is describing the energy loss of the fast electrons that propagate inside the material. The energy loss spectrum of $SrRhO_3$ is depicted in Figure 13c. Energy loss for $SrRhO_3$ is high along the whole spectrum and it is identical with intra + inter and intra band transition in the high energy region. We observe some peaks, the highest peaks are related to the plasma frequency [50]. From these Figures, the plasma frequency of $SrRhO_3$ occurs at 10.9 eV and 13.2 eV.

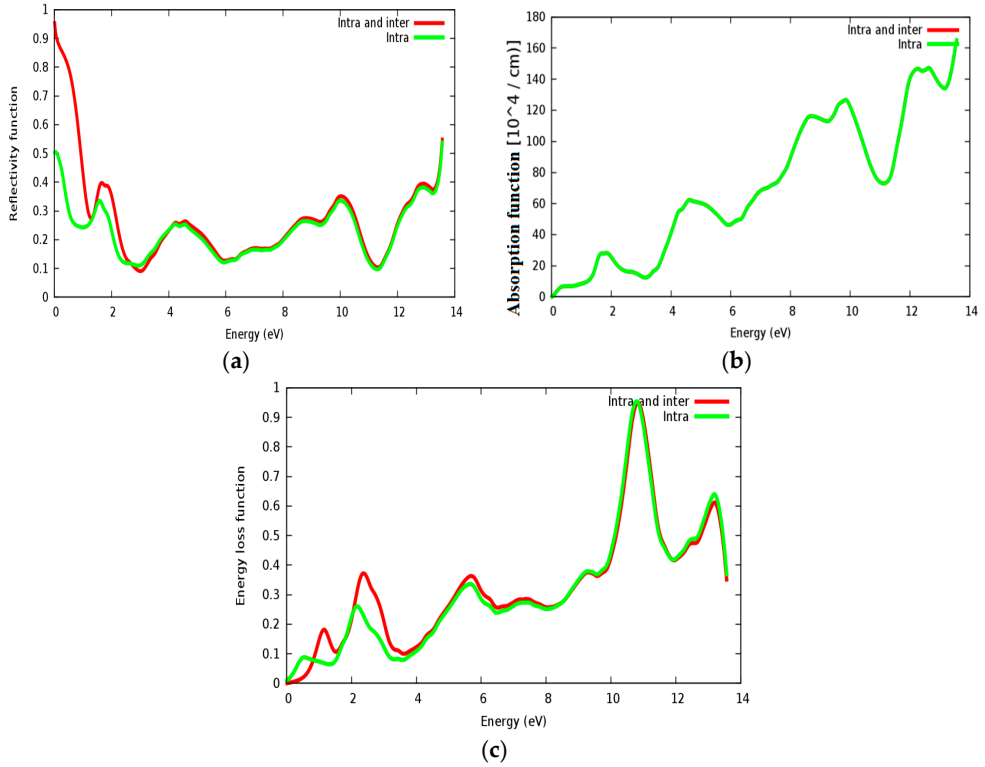

Figure 13. (**a**) Reflectivity function $R(\omega)$; (**b**) absorption function; and (**c**) energy loss function $L(\omega)$ for $SrRhO_3$ compound.

Figure 14a,b displays the calculated real and imaginary parts of the dielectric function for the $SrZrO_3$ compound for a radiation up to 14 eV. It is seen that the calculated linear optical components $\varepsilon_1(\omega)$ and $\varepsilon_2(\omega)$ spectra for $SrZrO_3$ are different from $SrRhO_3$. The calculated $\varepsilon_2(\omega)$ spectra show that the first critical point (threshold energy) of the dielectric function occurs at about 4.52 eV within the mBJ approach (GGA: 3.6 eV) for $SrZrO_3$; the first critical points are comparable with the energy band gap computed from the energy band structure. We can see from Figure 14b, that $\varepsilon_2(\omega)$ displaced to the high energy region within the mBJ approach, but the first peak in $\varepsilon_2(\omega)$ within the GGA approach has a higher value. The threshold's energy is followed by some peaks that originate from direct optical

transition between the valence band and conduction bands. The main peak in the absorptive spectra is positioned at about 7.2 eV within mBJ (GGA: 6.2 eV). The real part $\varepsilon_1(\omega)$ gives us information about the material's polarizability; the static dielectric constant $\varepsilon_1(0)$ of $SrZrO_3$ is 3 within the mBJ approach (GGA: 3.92), as we can see that the mBJ approach has a lower value of $\varepsilon_1(0)$. The value of $\varepsilon_1(\omega)$ within mBJ displaced to the higher energy region along the spectrum. The behavior with the high dielectric constant makes $SrZrO_3$ a possible useful candidate for manufacturing high capacitors [51]. The negative value in the spectra of $\varepsilon_1(\omega)$ for the $SrZrO_3$ compound is located only in the ultraviolet spectrum; and shows the metallic behavior of this compound in the mentioned region.

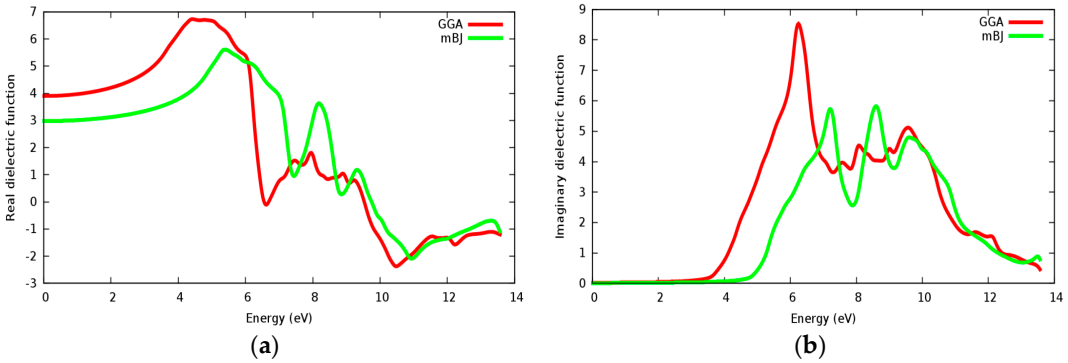

Figure 14. Dielectric function for $SrZrO_3$: (**a**) Real part; (**b**) Imaginary part using both PBE-GGA and mBJ-GGA methods.

In Figure 15a,b, the real and imaginary parts of conductivity are illustrated for $SrZrO_3$, respectively. It can be seen from Figure 15a, that the real part of conductivity starts to have considerable values at about 4.75 eV within the mBJ approach (GGA: 3.6 eV). From the conductivity and imaginary part of the dielectric function spectrums (Figure 14b), it is shown that both of them start to have a considerable value from approximately the same value. We have also observed some peaks in the conductivity spectra as also observed in the $\varepsilon_2(\omega)$ spectra. The conductivity increases as the material becomes more photon (energy) absorbent.

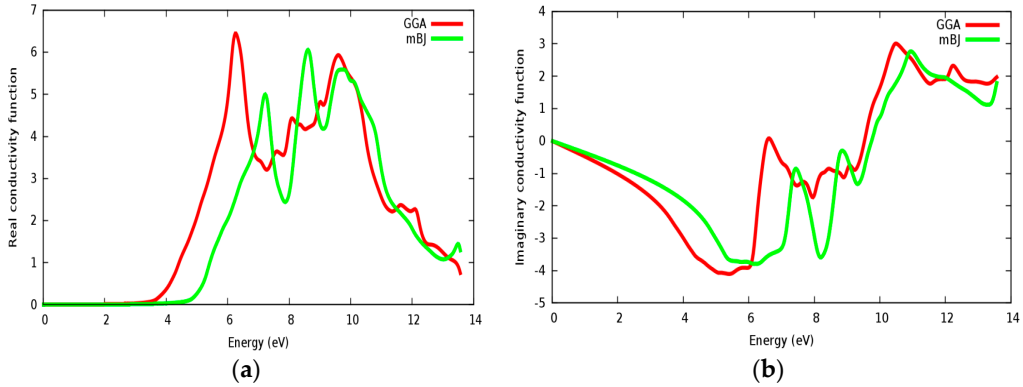

Figure 15. Conductivity function for $SrZrO_3$: (**a**) Real part; (**b**) Imaginary part using both PBE-GGA and mBJ-GGA methods.

Figure 16a,b displaying the extinction coefficient and refractive index $n(\omega)$. One can remark that the extinction coefficient of $SrZrO_3$ starts to have considerable value at 4.75 eV within mBJ (GGA: 3.6 eV). We can clearly see that $k(\omega)$, conductivity and $\varepsilon_2(\omega)$ start to have considerable values at the same point. Some peaks are presented along the spectrum, these peaks are related to the electrons transitions from valence to conduction bands. It is clearly seen that the extinction coefficient and the imaginary part of the epsilon vary in the same way. The static value of the refractive index $n(0)$ in

Figure 16b for the $SrZrO_3$ compound is 1.75 within the mBJ approach (GGA: 1.9), which is a small value compared to $n(0)$ for the $SrRhO_3$ compound.

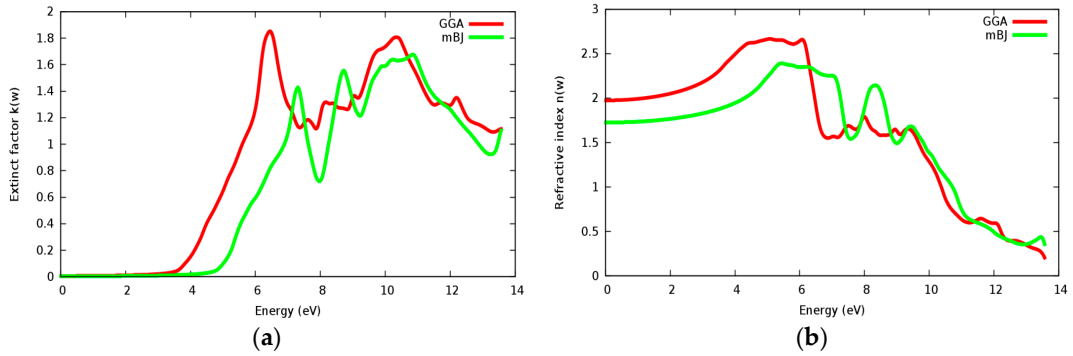

Figure 16. (**a**) Extinct factor $k(\omega)$; (**b**) Refractive index $n(\omega)$ for $SrZrO_3$ compound using both PBE-GGA and mBJ-GGA methods.

Reflectivity, energy loss and absorption functions are illustrated in Figure 17a–c, respectively. The static reflectivity of $SrZrO_3$ is about 0.07 within the mBJ approach (GGA: 0.11). The static reflectivity of $SrRhO_3$ is more than nine times greater than the reflectivity of $SrZrO_3$. The reflectivity value increases rapidly in the high energy region; far ultraviolet region (FUV); $ab = nd$ for the $SrZrO_3$ compound, indicating that $SrZrO_3$ is suitable as a wave reflectance compound in the far ultraviolet region (FUV). Energy loss and absorption functions are seen in Figure 17b,c; both of them quietly behave in the same way. Both absorption and energy loss for SrZrO3 begin at about 4.8 eV within the mBJ approach (GGA: 3.8 eV). The $SrZrO_3$ is a good absorbent compound, but not in the low energy region; it is good absorbent in the far ultraviolet region, as it shows metallic behavior in the high energy region.

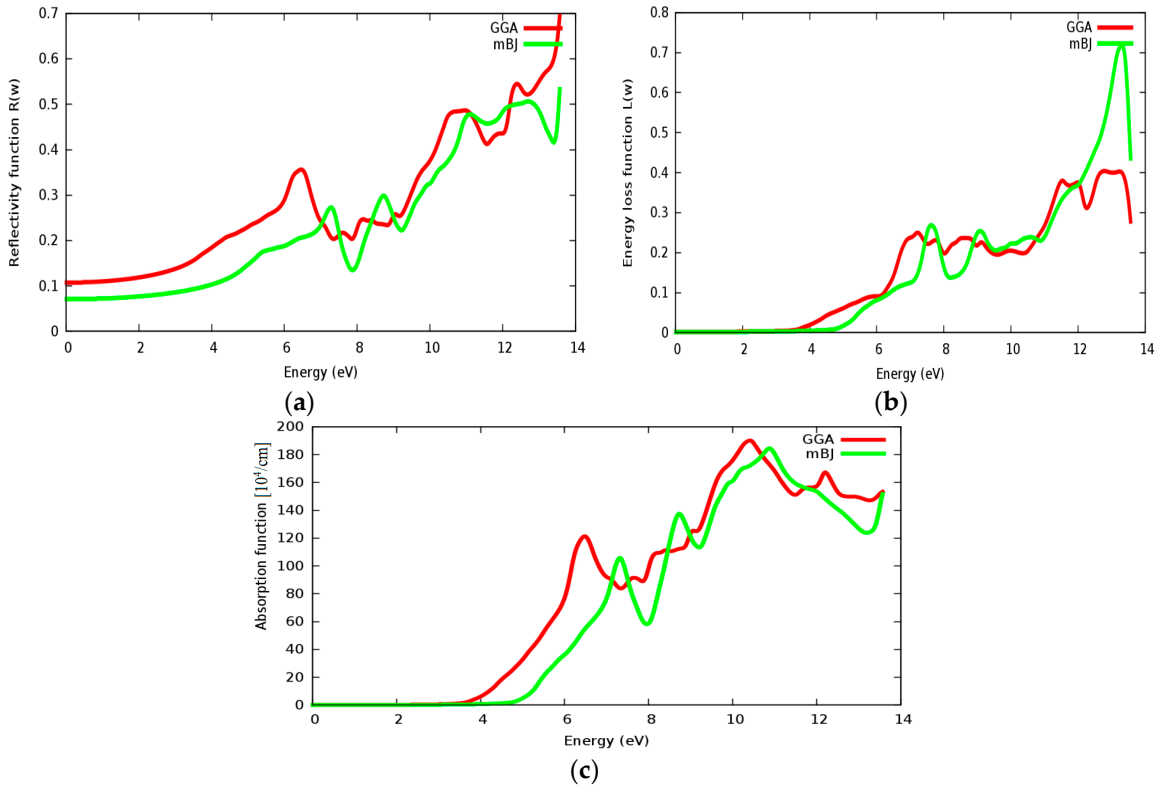

Figure 17. (**a**) Reflectivity function $R(\omega)$; (**b**) Energy loss function $L(\omega)$ and (**c**) absorption function for $SrZrO_3$ compound using both PBE-GGA and mBJ-GGA methods.

4. Conclusions

In summary, we have studied the structural, electronic, elastic and optical properties of $SrTMO_3$ (TM = Rh, Zr) using the FP-LAPW method within the PBE-GGA and mBJ-GGA approaches in the framework of density functional theory. The lattice parameter is found to be in good agreement with experimental and theoretical results. From the band structure, we found that the $SrRhO_3$ compound has a metallic nature within both BPE-GGA and mBJ-GGA approaches, while $SrZrO_3$ is found to be an insulator within mBJ-GGA, while it is a wide energy band gap semiconductor within PBE-GGA. The elastic constants (C_{11}, C_{12}, C_{44}), bulk modulus, shear modulus and Young's modulus are also calculated and discussed. By analyzing the B/S ratio and Poisson's ratio, we found that $SrRhO_3$ has a ductile nature, while $SrZrO_3$ has brittle nature. $SrZrO_3$ has a more ionic trend compared to the $SrRhO_3$. The optical properties such as dielectric constant, absorption coefficient, reflectivity coefficient, refractive index, optical conductivity and energy loss function were investigated in the energy range (0–14) eV. According to the dielectric constant, $SrZrO_3$ has a large static dielectric constant which may make it promising as a good dielectric material; while $SrRhO_3$ has a negative real dielectric constant which indicates a metallic behavior. It would be interesting to make detailed measurements of the transport and thermodynamic properties of $SrRhO_3$ under applied fields looking for metamagnetic behavior and non-Fermi-liquid scalings. In conclusion, our theoretical calculations on $SrTMO_3$ (TM = Rh, Zr) will help to use these materials for practical applications.

Author Contributions: Conceptualization, M.A.-J.; Data Curation, A.S., T.O. and A.M.; Formal Analysis, A.S., R.T.J. and T.O.; Investigation, M.A.-J. and R.K.; Methodology, M.A.-J.; Project Administration, M.A.-J.; Supervision, M.A.-J.; Visualization, M.A.-J.; Writing–Original Draft, A.S., T.O. and A.M.; Writing–Review & Editing, R.K. and K.F.I.

Funding: This research received no external funding.

Acknowledgments: This work has been carried out in the Computational Physics Laboratory, Physics Department, An-Najah N. University.

Conflicts of Interest: The funders had no role in the design of the study; in the collection, analyses, or interpretation of data; in the writing of the manuscript, and in the decision to publish the results.

References

1. Bouadjemi, B.; Bentata, S.; Abbad, A.; Benstaali, W.; Bouhafs, B. Half-metallic ferromagnetism in $PrMnO_3$ perovskite from first principles calculations. *Solid State Commun.* **2013**, *168*, 6–10. [CrossRef]
2. Rahaman, M.Z.; Rahman, M.A.; Sarker, M.A.R. Prediction of a new transition metal oxide $MgRhO_3$ with $SrTiO_3$-type structure: Stability, structure and physical characteristics Chin. *J. Phys.* **2017**, *55*, 1489–1494.
3. Yamaura, K.; Huang, Q.; Young, D.P.; Arai, M.; Takayama-Muromachi, E. Electronic properties of the novel 4d metallic oxide SrRhO3. *Phys. B Phys. Condens. Matter* **2003**, *329–333*, 820–821. [CrossRef]
4. Saha, S.; Sinha, T.P.; Mookerjee, A. Structural and optical properties of paraelectric $SrTiO_3$. *J. Phys. Condens. Matter* **2000**, *12*, 3325. [CrossRef]
5. Johnsson, M.; Lemmens, P. Crystallography and chemistry of perovskites. In *Handbook of Magnetism and Advanced Magnetic Materials*; Kronmüller, H., Parkin, S., Eds.; John Wiley & Sons: Hoboken, NJ, USA, 2007.
6. Pena, M.A.; Fierro, J.L. Chemical structures and performance of perovskite oxides. *Chem. Rev.* **2001**, *101*, 1981–2018. [CrossRef] [PubMed]
7. Ghebouli, B.; Ghebouli, M.A.; Chihi, T.; Fatmi, M.; Boucetta, S.; Reffas, M. First-principles study of structural, elastic, electronic and optical properties of $SrMO_3$ (M = Ti and Sn). *Solid State Commun.* **2009**, *149*, 2244–2249. [CrossRef]
8. Sakhya, A.; Maibam, J.; Saha, S.; Chanda, S.; Dutta, A.; Sharama, B.; Thapa, R.K.; Sinha, T.B. Electronic structure and elastic properties of $ATiO_3$ (A = Ba, Sr, Ca) perovskites: A first principles study. *Indian J. Pure Appl. Phys.* **2015**, *53*, 102–109.
9. Van Roosmalen, J.A.M.; van Vlaanderen, P.; Cordfunke, E.H.P. On the structure of $SrZrO_3$. *J. Solid State Chem.* **1992**, *101*, 59–65. [CrossRef]

10. Boudali, A.; Khodja, M.D.; Amrani, B.; Bourbie, D.; Amara, K.; Abada, A. First-principles study of structural, elastic, electronic, and thermal properties of $SrTiO_3$ perovskite cubic. *Phys. Lett. A* **2009**, *373*, 879–884. [CrossRef]
11. Blaha, P.; Schwarz, K.; Madsen, G.K.H.; Kvasnicka, D.; Luitz, J. *WIEN2k: An Augmented Plane Wave plus Local Orbitals Program for Calculating Crystal Properties*; Vienne University of Technology: Vienna, Austria, 2001.
12. Daga, A.; Sharma, S.; Sharma, K.S. First principle study of cubic $SrMO_3$ perovskites (M = Ti, Zr, Mo, Rh, Ru). *J. Mod. Phys.* **2011**, *2*, 812–816. [CrossRef]
13. Ali, M.L.; Rahaman, M.Z. The structural, elastic, electronic and optical properties of cubic perovskite $SRVO_3$ compound: An ab initio study. *Int. J. Mater. Sci. Appl.* **2016**, *5*, 202–206.
14. Ali, M.L.; Rahaman, M.Z. Variation of the physical proprties of four transition metal oxides $SrTMO_3$ (TM = Rh, Ti, Mo, Zr) under pressure: An ab initio study. *J. Adv. Phys.* **2017**, *6*, 197–205. [CrossRef]
15. *CASTEP Guide. Materials Studio 8.0*; BIOVIA: San Diego, CA, USA, 2010; pp. 261–262.
16. Shende, R.V.; Krueger, D.S.; Rosetti, G.A.; Lombardo, S.J. Strontium zirconate and strontium titanate ceramics for high-voltage applications: Synthesis, processing, and dielectric properties. *J. Am. Ceram. Soc.* **2001**, *84*, 1648–1650. [CrossRef]
17. Singh, D.J. Prospects for quantum criticality in perovskite $SrRhO_3$. *Phys. Rev. B* **2003**, *67*, 054507. [CrossRef]
18. Blaha, P.; Schwarz, K.; Sorantin, P.; Trickey, S.B. Full-potential, linearized augmented plane wave programs for crystalline systems. *Comput. Phys. Commun.* **1990**, *59*, 399–415. [CrossRef]
19. Monkhorst, H.J.; Pack, J.D. Special points for Brillouin-zone integrations. *Phys. Rev. B* **1976**, *13*, 5188. [CrossRef]
20. Perdew, J.P.; Burke, K.; Ernzerhof, M. Generalized gradient approximation made simple. *Phys. Rev. Lett.* **1996**, *77*, 3865. [CrossRef] [PubMed]
21. Becke, A.; Johnson, E.R. A simple effective potential for exchange. *J. Chem. Phys.* **2006**, *124*, 221101. [CrossRef] [PubMed]
22. Murnaghan, F.D. The compressibility of media under extreme pressures. *Proc. Natl. Acad. Sci. USA* **1944**, *30*, 244–247. [CrossRef] [PubMed]
23. Lee, Y.S.; Lee, J.S.; Noh, T.W.; Byun, D.Y.; Yoo, K.S.; Yamaura, K.; Takayama-Muromachi, E. Systematic trends in the electronic structure parameters of the 4*d* transition-metal oxides $SrMO_3$ (M = Zr, Mo, Ru, and Rh). *Phys. Rev. B* **2003**, *67*, 113101. [CrossRef]
24. Smith, A.J.; Welch, A.J.E. Some mixed metal oxides of perovskite structure. *J. Acta Crystallogr.* **1960**, *13*, 653–656. [CrossRef]
25. Ligny, D.D.; Richet, P. High-temperature heat capacity and thermal expansion of $SrTiO_3$ and $SrZrO_3$ perovskites. *Phys. Rev. B* **1996**, *53*, 3013. [CrossRef]
26. Mete, A.; Shaltaf, R.; Ellialtioglu, S. Electronic and structural properties of a 4*d* perovskite: Cubic phase of $SrZrO_3$. *Phys. Rev. B* **2003**, *68*, 035119. [CrossRef]
27. Bader, R.F.W. *Atoms in Molecules: A Quantum Theory*; Oxford University Press: Oxford, UK, 1990.
28. Luana, V.; Costales, A.; Pendas, A.M. Ions in crystals: The topology of the electron density in ionic materials. II. The cubic alkali halide perovskites. *Phys. Rev. B* **1997**, *55*, 4285. [CrossRef]
29. Mori-Sánchez, P.; Pendás, A.M.; Luaña, V. A classification of covalent, ionic, and metallic solids based on the electron density. *J. Am. Chem. Soc.* **2002**, *124*, 14721–14723. [CrossRef]
30. Becke, A.D.; Edgecombe, K.E. A simple measure of electron localization in atomic and molecular systems. *J. Chem. Phys.* **1990**, *92*, 5397–5403. [CrossRef]
31. Sun, Z.; Music, D.; Ahuja, R.; Schneider, J.M. Electronic origin of shearing in M_2AC (M = Ti, V, Cr, A = Al, Ga). *J. Phys. Condens. Matter* **2005**, *17*, 7169–7176. [CrossRef]
32. IRelast Package. Cubic-elastic_13.2; Part of the Commercial Code WIEN2k. Available online: http://susi.theochem.tuwien.ac.at/ (accessed on 1 September 2018).
33. Born, M. On the stability of crystal lattices. I. *Math. Proc. Camb. Philos. Soc.* **1940**, *36*, 160–172. [CrossRef]
34. Born, M.; Huang, K. *Dynamical Theory of Crystal Lattices*; Oxford University Press: Oxford, UK, 1956.
35. Hill, R. The elastic behaviour of a crystalline aggregate. *Proc. Phys. Soc. Sect. A* **1952**, *65*, 349. [CrossRef]
36. Voigt, W. *Lehrbuch der Kristallphysik (mit Ausschluss der Kristalloptik)*; B.G. Teubner: Berlin, Germany, 1910; pp. 1850–1919.
37. Reuss, A. Berechnung der fließgrenze von mischkristallen auf grund der plastizitätsbedingung für einkristalle. *Z. Angew. Math. Mech.* **1929**, *9*, 49–58. [CrossRef]

38. Terki, R.; Feraoun, H.; Bertrand, G.; Aourag, H. Full potential calculation of structural, elastic and electronic properties of $BaZrO_3$ and $SrZrO_3$. *Basic Solid State Phys.* **2005**, *242*, 1054–1062. [CrossRef]
39. Teter, D.M. Computational alchemy: The search for new superhard materials. *MRS Bull.* **2013**, *23*, 22–27. [CrossRef]
40. Pugh, S.F. XCII. Relations between the elastic moduli and the plastic properties of polycrystalline pure metals. *Philos. Mag.* **1954**, *45*, 823–843. [CrossRef]
41. Pettifor, D.G. Theoretical predictions of structure and related properties of intermetallics. *Mater. Sci. Technol.* **1992**, *8*, 345. [CrossRef]
42. Frantsevich, I.N.; Voronov, F.F.; Bokuta, S.A. *Elastic Constants and Elastic Moduli of Metals and Insulators Handbook*; Frantsevich, I.N., Ed.; Naukova Dumka: Kiev, Ukraine, 1983; p. 60.
43. Zener, C. *Elasticity and Anelasticity of Metals*; University of Chicago Press: Chicago, IL, USA, 1948.
44. Tvergaard, V.; Hutshinson, J.W. Microcracking in ceramics induced by thermal expansion or elastic anisotropy. *J. Am. Ceram. Soc.* **1988**, *71*, 157–166. [CrossRef]
45. Ehrenreich, H.; Cohen, M.H. Self-consistent field approach to the many-electron problem. *Phys. Rev.* **1959**, *115*, 786. [CrossRef]
46. Hedin, L. New Method for Calculating the One-Particle Green's function with application to the electron-gas problem. *Phys. Rev. A* **1965**, *139*, A796. [CrossRef]
47. Fox, M. *Optical Properties of Solids*; Oxford University Press: Oxford, UK, 2001.
48. Abeles, F. *Optical Properties of Solids*; American Elsevier: Atlanta, GA, USA, 1972.
49. Wang, H.; Wang, Y.; Cao, X.; Zhang, L.; Feng, M.; Lan, G. Simulation of electronic density of states and optical properties of PbB_4O_7 by first-principles DFT method. *Phys. Status Solidi B* **2009**, *246*, 437–443. [CrossRef]
50. He, Y.; Zeng, T. First-principles study and model of dielectric functions of silver nanoparticles. *J. Phys. Chem. C* **2010**, *114*, 18023–18030. [CrossRef]
51. Koontz, R.; Blokhina, G.; Gold, S.; Krasnykh, A. High dielectric constant materials for pulsed energy storage capacitors. In Proceedings of the 1998 Annual Report Conference on Electrical Insulation and Dielectric Phenomena (Cat. No. 98CH36257), Atlanta, GA, USA, 25–28 October 1998.

© 2018 by the authors. Licensee MDPI, Basel, Switzerland. This article is an open access article distributed under the terms and conditions of the Creative Commons Attribution (CC BY) license (http://creativecommons.org/licenses/by/4.0/).